Nanoscale

PAPER

View Article Online
View Journal | View Issue

Cite this: *Nanoscale*, 2019, **11**, 11626

Rapid dry exfoliation method for tuneable production of molybdenum disulphide quantum dots and large micron-dimension sheets†

Mustafa Ahmed, Heba Ahmed, Amgad R. Rezk and Leslie Y. Yeo *

Despite advances in two-dimensional (2D) transition metal dichalcogenide research owing to their outstanding physical properties, the synthesis of large micron-dimension single-layer sheets of these materials remains a challenge. Here, we present a novel and unique method to rapidly and flexibly exfoliate bulk molybdenum disulphide (MoS_2) into either small nanometre-dimension quantum dots (QDs) or large micron-dimension sheets comprising predominantly single- or few-layers. The exfoliation process is conducted in dry phase, *i.e.*, without liquid, by exploiting nanometer-amplitude MHz-order surface vibrations in the form of surface acoustic waves (SAWs). To produce the small QDs, we take advantage of the unprecedentedly large surface acceleration—on the order of 10^8 m s^{-2}—to induce an iterative impaction mechanism involving successive ejection and collision of the bulk MoS_2 aggregates within a miniature enclosure in order to progressively thin and break their lateral dimensions into single- and few-layer QDs. In contrast, we suppress the impaction in the zero-height enclosure limit by confining the bulk MoS_2 under adhesive tape such that the shear that arises due to the travelling SAW on the substrate progressively thins the material whilst preserving their lateral dimension such that large, predominantly-monolayer, micron-sized sheets are produced with high substrate coverage up to around 80%. This fast, additive-free and dry exfoliation platform potentially presents a simple yet scalable micromechanical exfoliation method towards viable commercial production of 2D transition metal dichalcogenides.

Received 18th May 2019,
Accepted 1st June 2019

DOI: 10.1039/c9nr04255e

rsc.li/nanoscale

1. Introduction

In spite of the well-documented properties of 2D MoS_2 and, in general, other transition metal dichalcogenides,[1–7] the practical adoption of these materials in commercial applications largely depends on the fabrication process by which they are synthesized. In particular, the lateral dimension of exfoliated MoS_2 can vary hugely from large micron-scale sheets to small nano-scale QDs, and their thicknesses from predominantly single to several layers. The earliest exfoliation methods involved their peeling with the aid of adhesive tape,[8–14] which offers a way to attain pristine micron dimension sheets down to single layer thicknesses. Nevertheless, despite its simplicity, the peeling process, in addition to being rather time-consuming, is extremely skill-dependent, therefore offering very little run-to-run reproducibility of the flake dimensions and thicknesses. More recent developments involving mechanical exfoliation have facilitated higher yield synthesis of sheets that are several hundreds of microns in dimension and allow their transfer onto a specific substrate desired for a particular application, albeit at the expense of introducing complexity, the need for additives that often contain aggressive etchants, and the lack of tuneability or scaleability.[14] As such, considerable effort has since been dedicated to the development of alternative methods to exfoliate these materials, which can be broadly categorised into either bottom-up or top-down approaches.

In bottom-up approaches, monolayers or few-layers of the 2D crystal are grown on a substrate, primarily by physical or chemical vapor deposition (PVD/CVD). Although adequately pristine 2D crystals are obtained,[15–18] it is often challenging to transfer the crystals from the substrate they are grown on during production onto the desired substrate.[18–20] An alternative technique involving direct sulphurisation of a deposited thin metal oxide layer[19,21–24] circumvents the need for such substrate transfer, but adds further complexity to an already slow and expensive process, in which the fabrication parameters are tightly correlated with both the substrate on which the material is to be grown, as well as the material itself, and thus have to be finely tuned for each fabrication procedure.[25–27]

Top-down approaches, on the other hand, typically involve agitating a liquid suspension of the material at high speeds, *via* high-shear mixing in a blender,[28–30] electrochemical exfoliation,[31] ultrasonication[32–37] or acoustofluidic microcentrifu-

Micro/Nanophysics Research Laboratory, RMIT University, Melbourne, VIC 3000, Australia. E-mail: leslie.yeo@rmit.edu.au

†Electronic supplementary information (ESI) available. See DOI: 10.1039/C9NR04255E

gation,[38] for example, to drive shearing of its bulk phase into exfoliated 2D crystals. The processing time, however, ranges from several to even a hundred hours, especially if the monolayer yield is to be increased.[30,32,37,39,40] Paradoxically, the longer the shearing process to acquire more crystals that are in monolayer form, the greater the tendency to break the material laterally. Consequently, the 2D crystals that are usually produced with these methods typically comprise nanosheets with lateral dimensions in the order of tens of nanometres, or QDs with lateral dimensions below 15 nm.[27,30] As such, the production of large sub-micron or micron dimension sheets is considerably challenging with these methods. Moreover, liquid exfoliation methods usually employ solvents as intercalating agents to enhance the exfoliation process,[32,34,35,37,41,42] although their use affects the quality of the exfoliated material and often poses considerable safety hazards particularly for large scale production, given that the typical solvents that are conventionally used, with the exception of a few recent methods employing pure water,[43,44] tend to be volatile, flammable, corrosive and toxic. Other surfactant additives or binary solvents are often employed to prevent restacking of the MoS_2 layers,[33,45] although their use are also generally known to affect product purity. While binary solvents or thermally-controlled water as a liquid medium have been used to mitigate the effect of these additives,[46,47] the adsorbed solvents are still known to affect the quality of the synthesized material.[27]

There have since been efforts, albeit limited, to circumvent the problems associated with liquid-phase exfoliation using dry grinding and milling;[48] these methods, however, still result in typically smaller lateral sheet sizes on the order of tens of nanometres[48] and require the addition of bulking and abrasive agents such as NaCl, which lead to contamination of the final product and hence necessitate subsequent use of a solvent for their separation. Whichever the method, wet or dry, the challenge nevertheless remains in obtaining contaminant-free and pristine larger sheets with sizes beyond 200 nm in lateral dimension.

Here, we attempt to address the aforementioned challenges associated with bottom-up approaches by developing a dry (solvent- and additive-free) technique that is able to synthesize relatively large micron-dimension MoS_2 sheets, or, alternatively, smaller nanoscale QDs, with acceptable monolayer yields. In either case, a dry, stable powder of exfoliated product that is free from additives and that does not restack—a problem generally associated with exfoliation involving liquid suspensions—is obtained. The method builds upon our recent work demonstrating the possibility of utilising surface acoustic waves (SAWs)—nanometre amplitude electromechanical waves that propagate along the surface of a piezoelectric substrate[49,50]—to efficiently exfoliate bulk transition metal dichalcogenides into either monolayer or few-layer 30 nm dimension nanosheets[51] or QDs[52] through a microfluidic nebulisation process. However, unlike these liquid-phase precedents, wherein the remarkably large substrate acceleration associated with the SAW—on the order 10^8 m s^{-2} (ref. 53–55)—was exploited to drive the nebulisation of a liquid suspension of the bulk material to induce its exfoliation, we harness this extremely potent mechanism to instead supply the mechanical shear and impact forces necessary to drive the exfoliation process in dry solid phase. We shall show, in stark contrast, that this not only allows comparably thin (monolayer to few-layers), albeit significantly larger, micron-sized MoS_2 sheets to be produced, but also allows the tuneable possibility of synthesizing nanometre-dimension QDs—both without necessitating any liquid, including solvents and additives.

2. Materials & methods

The schematics in Fig. 1 provide an illustration of the experimental setup, comprising the single-crystal piezoelectric lithium niobate (128° *Y*-rotated, *X*-propagating $LiNbO_3$; Roditi Ltd, London, UK) chipscale substrate on which the SAW propagates. The SAW itself is generated by applying an oscillating electrical signal at resonance from a signal generator (SML01; Rhode & Schwarz, North Ryde, NSW, Australia) and amplifier (LYZ-22+; Mini Circuits, Brooklyn, NY, USA) to focussed interdigitated transducer electrodes (IDTs) consisting of sixty 5 mm-wide interleaved finger pairs with a gap and spacing that corresponds to one-eighth of the SAW wavelength λ = 132 μm and hence its resonant frequency ω = 30 MHz. The IDTs, which comprise single-phase unidirectional transducer (SPUDT) designs, wherein acoustic reflectors are inserted between the electrode fingers such that the SAW only propagates in the forward direction (*i.e.*, the waves constructively interfere in the forward direction and destructively in the reverse), were patterned onto the chip by sputter coating (SPI-Module Sputter Coater; Structure Probe Inc., West Chester, PA, USA) a 10 nm chromium adhesion layer and a 500 nm aluminium layer onto the substrate, followed by etching using standard photolithography techniques.

Depending on whether nanoscale QDs or large micron sheets are desired, we either contained 5 mg of bulk MoS_2 powder (6 μm, 99.9% purity (US1089M, CAS: 1317-33-5); US Research Nanomaterials Inc., Houston, TX, USA) within a custom-made glass enclosure of dimensions 5 mm × 5 mm × 1 mm (Fig. 1(a, b)), or confined 1 mg of bulk MoS_2 powder under thermal adhesive tape (Graphene Square, Fort Lee, NJ, USA) and a 1 g load (Fig. 1(c, d)) prior to their excitation with the SAW. In the former, the input power was 1 mW prior to amplification with a 20% duty cycle (50 ms per 250 ms), whereas we employed either 0.05 mW or 0.2 mW subject to a 50% duty cycle (50 ms per 100 ms) in the latter; regular tape was also used in place of the thermal adhesive with no effect on the result, although this required an additional wash step with 45% ethanol after the exfoliation. To release the exfoliated particles from the tape in the latter case, we heat the device to 100 °C for 3 min. The particulate product comprising the exfoliated MoS_2 from either case was collected in a microcentrifuge tube (Eppendorf South Pacific Pty. Ltd, North Ryde, NSW, Australia) and suspended in 1 ml 45% ethanol in deionised water (18.2 MΩ cm, Milli-Q; MerckMillipore, Bayswater, VIC,

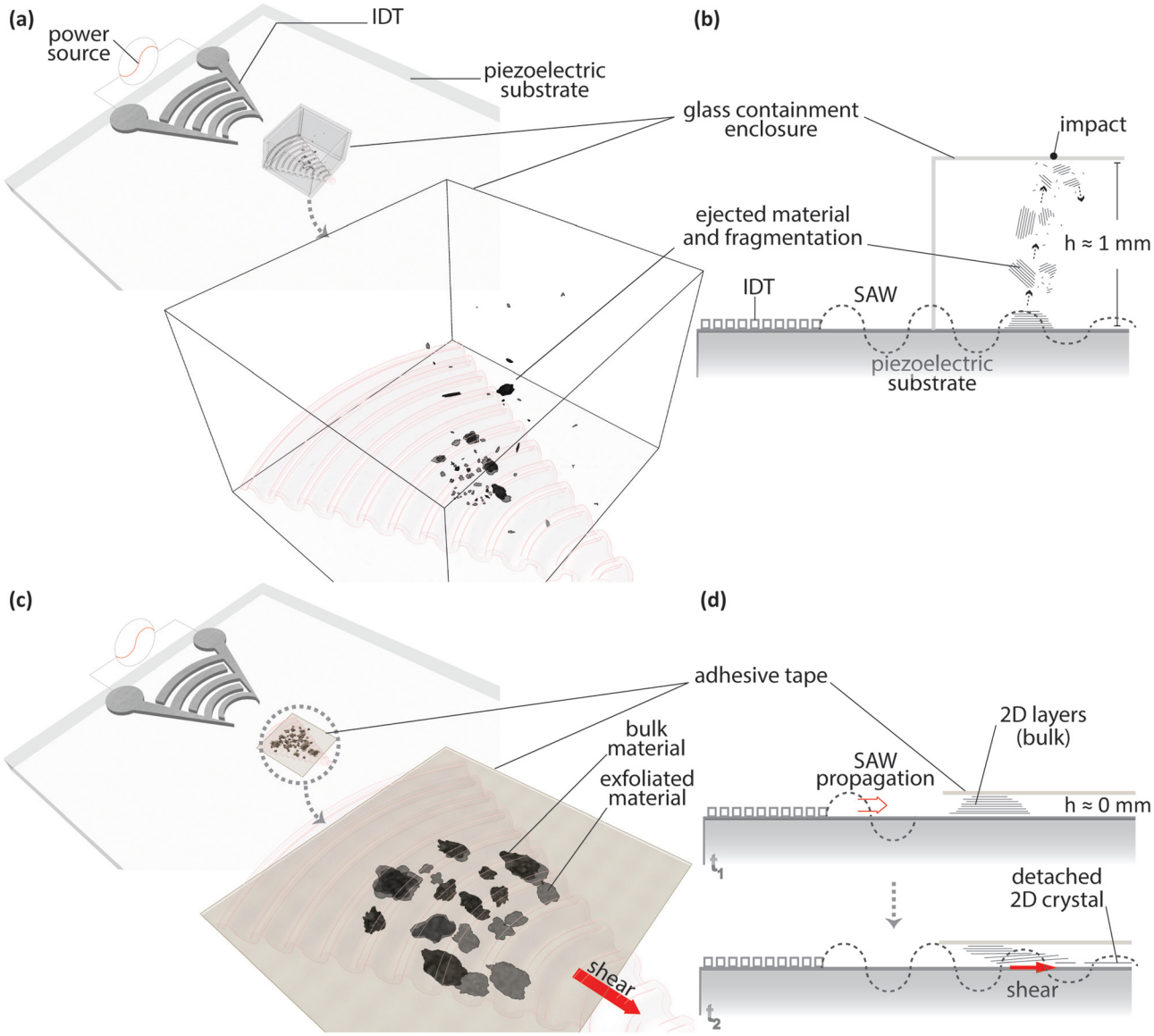

Fig. 1 Schematic depiction of the device employed for dry exfoliation of MoS_2 in which two configurations of the experimental setup were explored. (a, b) Perspective and side view illustrations of the setup in which the bulk MoS_2 powder feedstock was contained within a glass enclosure and exfoliated into QDs *via* an impact mechanism involving multiple ejection–collision–settling cycles occurring within the enclosure due to the large SAW substrate acceleration. (c, d) Perspective and side view illustrations of the asymptotic zero-height-limit setup in which the bulk MoS_2 powder feedstock was confined under adhesive tape such that it is progressively delaminated into large micron-sized sheets by the shear arising due to the SAW propagation along the substrate surface.

Australia), prior to being centrifuged (10 000 rpm for 20 min in the former case and 2000 rpm for 5 min in the latter case) to separate the supernatant containing the exfoliated product from the remaining bulk material. We note that this final step involving collection in a solvent was only required for size fractionation for characterisation of the sample; collection of the exfoliated product powder in dry stable form is possible since they are not bound to the substrate.

The MoS_2 QDs or sheets that were collected were then deposited onto a mica substrate and dried overnight in vacuum at room temperature prior to Atomic Force Microscopy (AFM) imaging (Multimode 8 with PeakForce Tunneling (TUNA) module; Bruker Corp., Santa Barbara, CA, USA). For high resolution Transmission Electron Microscopy (HR-TEM; Tecnai F20, FEI, Hillsboro, OR, USA), the samples were instead dried at room temperature on a carbon grid, on which they were imaged under an accelerating voltage of 200 kV. AFM images were flattened at 0.5 nm *z*-threshold and the analyses to measure their thicknesses and lateral dimensions were carried out using the supplied software (NanoScope, v1.8; Bruker Corp., Santa Barbara, CA, USA). We analysed at least 100 particles per experimental condition for the QDs and over

800 particles for the large sheets. Powder X-ray diffraction (XRD) of exfoliated MoS_2 (D8 Advance, Bruker Pty. Ltd, Preston, VIC, Australia) with Cu Kα radiation at 40 mA and 40 kV (λ = 1.54 Å) at a scan rate of 2° min^{-1}, step size of 0.02° and a 2θ range of 6° to 90° on a glass substrate was compared to bulk powder data (Crystallography Open Database[56,57] information card entry 1010993 [58]). Raman spectroscopy of the exfoliated product was, on the other hand, carried out *via* excitation at 532 nm (10 mW, 370–420 cm^{-1} acquisition range, LabRAM HR Evolution; Horiba Ltd, Kyoto, Japan) whereas UV/Vis absorbance, photoluminescence (PL) and fluorescence measurements were performed using a quartz cuvette (10 mm path length, FireFlySci 701MFL; Quark Photonics Pty. Ltd, Melbourne, VIC, AU) in a UV/Vis spectrophotometer (Cary 50 UV-Vis; Varian Inc., Santa Clara, CA, USA) and UV/Vis spectrofluorometer (Fluoromax-4P; Horiba Ltd, Kyoto, Japan).

3. Results & discussion

In the first configuration, *i.e.*, the production of QDs, the large particulates comprising the bulk MoS_2 feed in the enclosure were ejected from the substrate due to the tremendous $\mathcal{O}$ (10^8 m s^{-2}) surface acceleration that is generated on the substrate as the SAW traverses along it, subsequently colliding with the top and side walls of the enclosure (Fig. 1(a, b)) and settling before being re-ejected. This ejection–collision–settling sequence occurs over many cycles. The ejection and collision events initially fragment aggregates present in the bulk powder feedstock into clumps that are approximately on the order of 100 μm in dimension, consistent with that observed in previous work in which the large substrate acceleration associated with the SAW was exploited for the deagglomeration of carbon nanotube bundles[59]. As shown in Fig. 2 for two of the ejection–collision–settling cycles, it can be seen, however, that the repetitive events over many cycles lead to progressive fragmentation of the clumps beyond their deagglomeration, not just into individual flakes but also cleaving and thinning them down to monolayer and few-layer QDs. This is evident in the results shown in Fig. 3, where increasing the exposure time of the SAW excitation—which is commensurate to increasing the number of ejection and collision cycles, and hence impact events—can be seen to lead to dimensional reduction of the MoS_2. After just 100 ms (or around 50 impact events, assuming an in-flight velocity of 0.5 m s^{-1}, as estimated from high speed video images (ESI Fig. 1†)), we were able to obtain fairly monodispersed 10 nm QDs of which around 90% consisted of either monolayers or two-layers (Fig. 3(IV-d)).

Such impact-driven dimensional reduction is perhaps not surprising when the force experienced by a single MoS_2 flake during ejection is considered. For a substrate displacement amplitude ξ—estimated *via* laser Doppler vibrometry (UHF-120; Polytec Inc., Irvine, CA, USA)—of approximately 20 nm, we estimate a force $\rho L^2 h\omega^2\xi$ of approximately 100 nN, which is on the order of that required for rupture of MoS_2 flakes induced by an AFM tip;[60] here, ρ is the flake density, and, L and h are its lateral dimension and thickness, respectively. Moreover, the AFM scans in Fig. 3, as well as the PL intensity spectra in Fig. 4 (see also ESI Fig. 2(a)† where the data shows excitation at different wavelengths, exhibiting a progressive blue shift commensurate with a reduction in the dimensions of the material[61,62] with increasing SAW exposure duration) suggest the possibility for flexibly tuning the QD synthesis, both in terms of their height (*i.e.*, number of layers) and their lateral dimension, simply through modulation of the incredibly short millisecond-order exposure time. Further characterisation of the QDs with UV-Vis absorbance spectrometry can be found in ESI Fig. 2(b)† indicating the absorbance and overall collective PL behaviour of the QDs, powder XRD in ESI Fig. 3† indicating that the sample primarily comprises the 2H phase, HR-TEM in ESI Fig. 4† showing the sample size and crystallinity, and the data in ESI Fig. 5† showing the quantum yield increase with increasing SAW exposure duration.

The latter configuration, in which the bulk MoS_2 feed is confined beneath adhesive tape (Fig. 1(c, d)), on the other hand, constitutes the asymptotic limit of zero-enclosure-height wherein all impact events (*i.e.*, the ejection–collision–settling cycles) are suppressed. In this case, large MoS_2 sheets are produced in place of the QDs (Fig. 5). This is because the impaction mechanism in the former enclosure configuration in Fig. 1(a, b) primarily results in the reduction of the particulates in both dimensions, *i.e.*, the thickness as well as the lateral dimension. As seen by the resultant MoS_2 sheets in Fig. 5(a, b) (see also the HR-TEM image and the associated diffraction pattern of representative sheets in ESI Fig. 6†

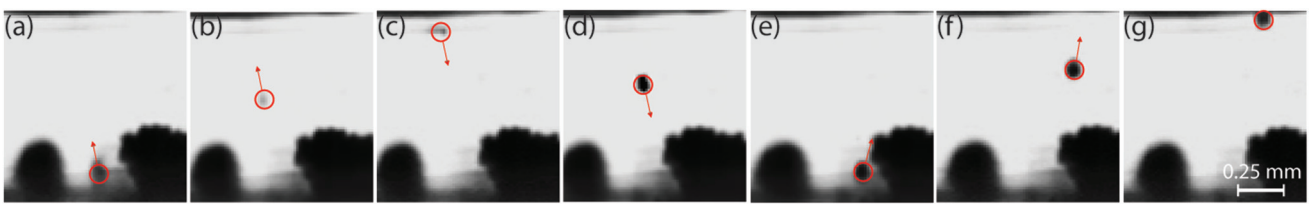

Fig. 2 Sequence of images captured by high speed videography depicting the dominant mechanism for the exfoliation of bulk MoS_2 within the containment enclosure illustrated in Fig. 1(a, b) for the production of QDs. (a–g) Two ejection–collision–settling cycle sequences over 6 ms in duration (1 ms increments between frames) wherein an MoS_2 powder cluster is progressively reduced in both height and lateral dimension upon impact with the walls of the enclosure.

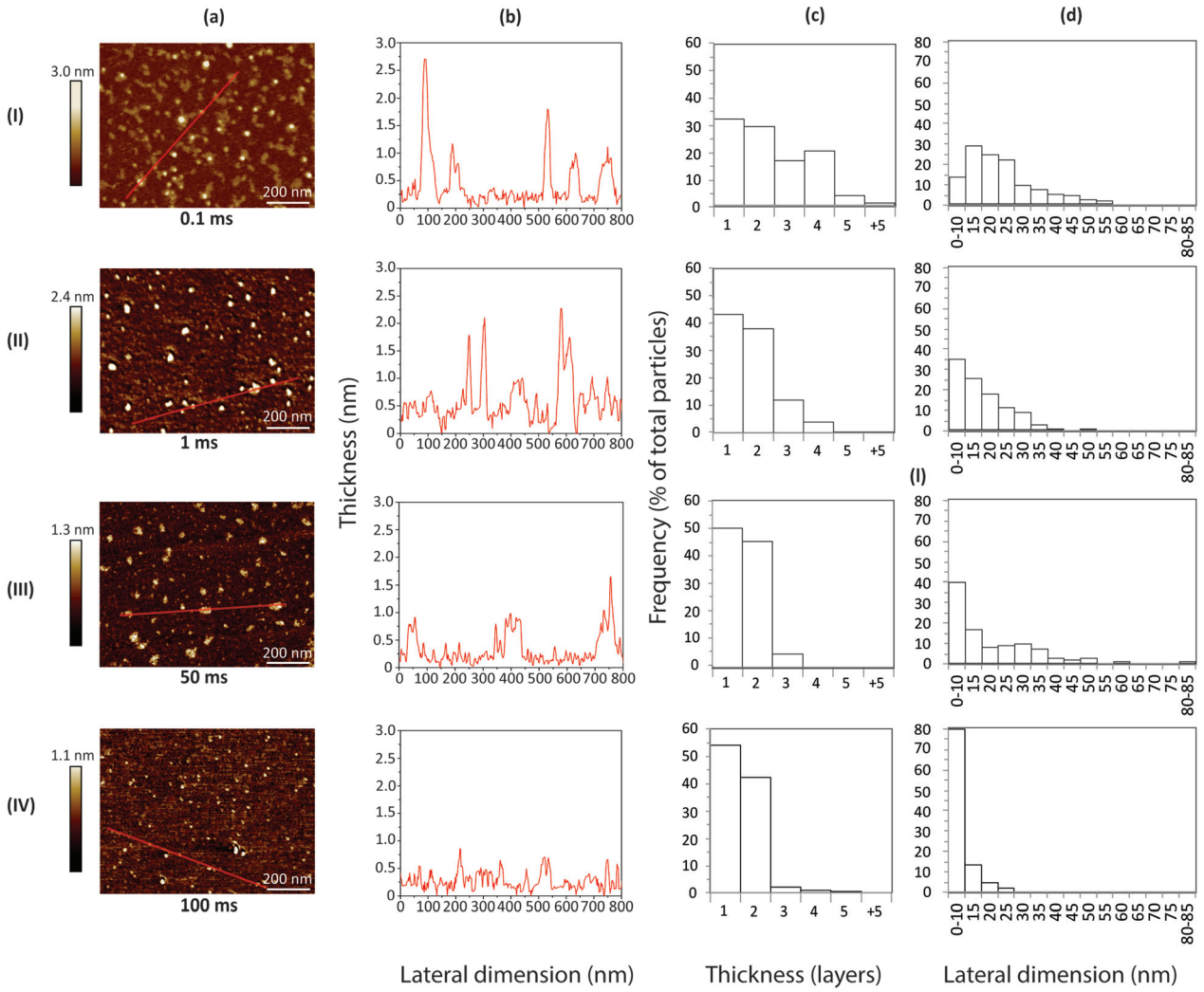

Fig. 3 (a) AFM scans and (b) height profiles, and, corresponding (c) thickness and (d) lateral dimension frequency distributions of the MoS_2 QDs produced under impaction through multiple ejection–collision–settling cycles within the enclosure (Fig. 1(a, b)) due to the large SAW substrate acceleration over different excitation times: (I) 0.1 ms, (II) 1 ms, (III) 50 ms, and, (IV) 100 ms.

showing the crystalline nature of the sheets), on the other hand, suppressing the impact by confining the sheets to the substrate, in contrast, allows the shear force that arises as a consequence of the SAW propagation along the substrate surface to dominate such that the stacked layers in the material are progressively delaminated whilst preserving their lateral dimensions, regardless of the starting thickness of the bulk material.

That travelling SAWs can give rise to sliding motion of a wide range of object sizes along the substrate surface, be it for relatively large millimeter-scale objects such as sliders,[63] micropropellers[64] or droplets,[65–70] or small sub-micron objects such as nanowires[71] and even sub-atomic particles such as excitons,[72] has previously been reported. In each of these, including the present case, the SAW acts as a conveyor belt that translates these objects along its propagation direction. By immobilising the topmost layer of the material to the adhesive tape in the present configuration (Fig. 1(c, d)), the moving

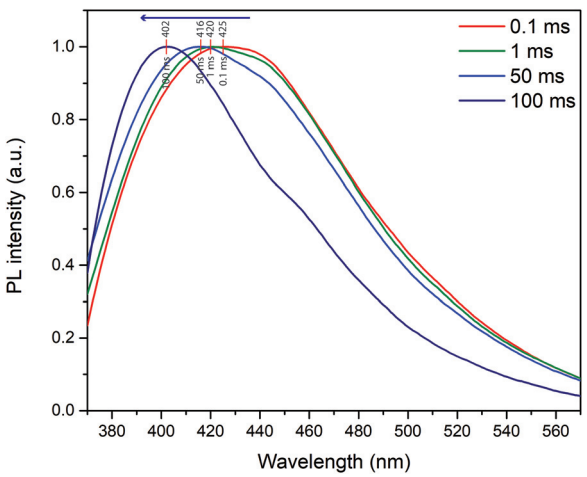

Fig. 4 Normalised PL spectra of the QDs produced in the enclosure setup depicted in Fig. 1(a, b) for increasing SAW exposure times. A blue-shift in the PL peak can be seen with increasing exposure duration.

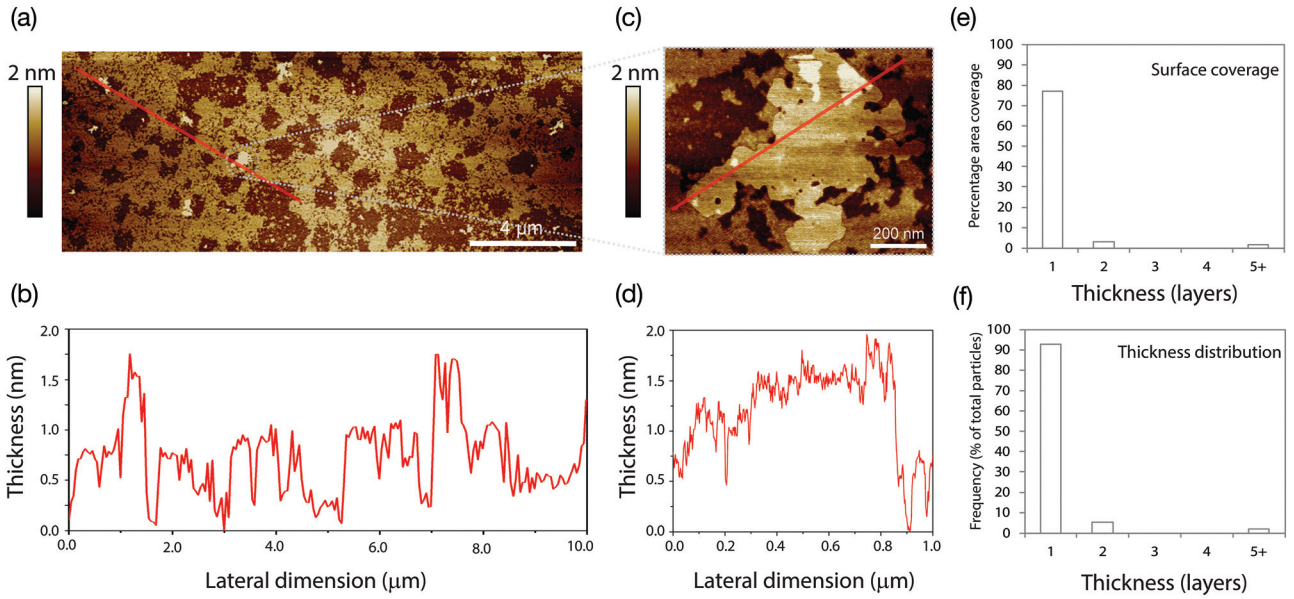

Fig. 5 (a, c) AFM scans and (b, d) height profiles of the large MoS_2 sheets produced due to the shear as a consequence of the travelling SAW in the zero-height-limit enclosure case by confining the feed under adhesive tape, as depicted in Fig. 1(c, d). The image and height profile in (c, d) is a magnification of one of the sheets found in (a, b). (e) Percentage surface area coverage and (f) sheet thickness in terms of the number of layers of each individual sheet.

surface beneath successively shears individual layers of the material adjacent to it as the travelling SAW propagates, and subsequently transports them away from the parent cluster, as depicted in the schematic in Fig. 1d. As their lateral dimensions are more or less preserved due to the suppression of the impact force, we observe this technique to remarkably result in large, pristine monolayer sheets (Fig. 5(a–d))—which is difficult to achieve with many other techniques.[27]

Moreover, it can be seen that the surface area coverage of the sheets, given in terms of the number of layers for each individual sheet in Fig. 5(e), is impressively large (≈80%), most of which comprise single-layer sheets with the exception of a few that are made up of two layers or more (Fig. 5(f)); the data has been compiled from a number of AFM images accounting for over 800 sheets, for which three sample images are shown in ESI Fig. 7(c).† We further characterised the exfoliated sheets through powder XRD and Raman spectroscopy (ESI Fig. 8(a, b)†) and show from the absorption spectra and corresponding excitonic peaks for four samples acquired for different SAW exposure durations and powers that the sheet concentration and yield can be tuned to some extent by increasing either the time or intensity over which the samples are exposed to the SAW (ESI Fig. 8(c)†), thus allowing the production rate of an already rapid exfoliation process to be increased. While the equivalent monolayer yield, obtained from the UV-Vis spectra, is relatively low (≈0.24%) for a single device, we note that the throughput can be dramatically increased through scaling out *via* device parallelisation, especially given the low cost of each device (≈US$1 by exploiting the economies of scale associated with mass nanofabrication) and the speed of the process.

4. Conclusion

In summary, we have demonstrated a novel chipscale platform for fast, dry (solvent- and additive-free) MoS_2 exfoliation that allows the synthesis of either small nanometre-scale QDs through an impaction mechanism involving repetitive ejection and collision events within an enclosure by taking advantage of the tremendous substrate acceleration associated with the SAW, or, in the zero-height-limit of the enclosure, large micron-dimension sheets with high surface coverage through a shearing mechanism. Further, we show that it is possible to tune the lateral dimension as well as the thickness down to monolayer QDs and sheets through the SAW power and exposure duration. Not only is the chemical nature of the material, *i.e.* MoS_2, maintained despite its exposure to the acoustic radiation,[73] the absence of any chemical additives preserves the quality of the end product, which is a significant advantage over other methods. Furthermore, the simplicity and low-cost of the process facilitates production intensification towards larger-scale yields through massive parallelisation of the miniaturised chip-scale setup.

Conflicts of interest

There are no conflicts to declare.

Acknowledgements

The authors are grateful for access and technical help associated with the use of the nanofabrication equipment in the

RMIT MicroNano Research Facility (MNRF). ARR and LYY acknowledge funding from the Australian Research Council (ARC) through Discovery Project DP180102110.

References

1 S. Ghatak, A. N. Pal and A. Ghosh, *ACS Nano*, 2011, **5**, 7707–7712.
2 B. Radisavljevic, A. Radenovic, J. Brivio, V. Giacometti and A. Kis, *Nat. Nanotechnol.*, 2011, **6**, 147–150.
3 H. S. Lee, S.-W. Min, Y.-G. Chang, M. K. Park, T. Nam, H. Kim, J. H. Kim, S. Ryu and S. Im, *Nano Lett.*, 2012, **12**, 3695–3700.
4 M. Chhowalla, H. S. Shin, G. Eda, L.-J. Li, K. P. Loh and H. Zhang, *Nat. Chem.*, 2013, **5**, 263–275.
5 M. M. Furchi, D. K. Polyushkin, A. Pospischil and T. Mueller, *Nano Lett.*, 2014, **14**, 6165–6170.
6 L. Wang, Y. Wang, J. I. Wong, T. Palacios, J. Kong and H. Y. Yang, *Small*, 2014, **10**, 1101–1105.
7 G.-B. Liu, D. Xiao, Y. Yao, X. Xu and W. Yao, *Chem. Soc. Rev.*, 2015, **44**, 2643–2663.
8 K. S. Novoselov, D. Jiang, F. Schedin, T. J. Booth, V. V. Khotkevich, S. V. Morozov and A. K. Geim, *Proc. Natl. Acad. Sci. U. S. A.*, 2005, **102**, 10451–10453.
9 A. Castellanos-Gomez, N. Agraït and G. Rubio-Bollinger, *Appl. Phys. Lett.*, 2010, **96**, 213116.
10 C. R. Dean, A. F. Young, I. Meric, C. Lee, L. Wang, S. Sorgenfrei, K. Watanabe, T. Taniguchi, P. Kim, K. L. Shepard and J. Hone, *Nat. Nanotechnol.*, 2010, **5**, 722–726.
11 H. Li, Z. Yin, Q. He, H. Li, X. Huang, G. Lu, D. W. H. Fam, A. I. Y. Tok, Q. Zhang and H. Zhang, *Small*, 2011, **8**, 63–67.
12 K. F. Mak, K. He, J. Shan and T. F. Heinz, *Nat. Nanotechnol.*, 2012, **7**, 494–498.
13 H. Li, J. Wu, Z. Yin and H. Zhang, *Acc. Chem. Res.*, 2014, **47**, 1067–1075.
14 S. B. Desai, S. R. Madhvapathy, M. Amani, D. Kiriya, M. Hettick, M. Tosun, Y. Zhou, M. Dubey, J. W. Ager III, D. Chrzan and A. Javey, *Adv. Mater.*, 2016, **28**, 4053–4058.
15 M. R. Laskar, L. Ma, S. Kannappan, P. Sung Park, S. Krishnamoorthy, D. N. Nath, W. Lu, Y. Wu and S. Rajan, *Appl. Phys. Lett.*, 2013, **102**, 252108.
16 S. Wu, C. Huang, G. Aivazian, J. S. Ross, D. H. Cobden and X. Xu, *ACS Nano*, 2013, **7**, 2768–2772.
17 W. Zhou, X. Zou, S. Najmaei, Z. Liu, Y. Shi, J. Kong, J. Lou, P. M. Ajayan, B. I. Yakobson and J.-C. Idrobo, *Nano Lett.*, 2013, **13**, 2615–2622.
18 A. L. Elías, N. Perea-López, A. Castro-Beltrán, A. Berkdemir, R. Lv, S. Feng, A. D. Long, T. Hayashi, Y. A. Kim, M. Endo, H. R. Gutiérrez, N. R. Pradhan, L. Balicas, T. E. Mallouk, F. López-Urías, H. Terrones and M. Terrones, *ACS Nano*, 2013, **7**, 5235–5242.
19 J.-G. Song, J. Park, W. Lee, T. Choi, H. Jung, C. W. Lee, S.-H. Hwang, J. M. Myoung, J.-H. Jung, S.-H. Kim, C. Lansalot-Matras and H. Kim, *ACS Nano*, 2013, **7**, 11333.
20 Y. Zhang, Y. Zhang, Q. Ji, J. Ju, H. Yuan, J. Shi, T. Gao, D. Ma, M. Liu, Y. Chen, X. Song, H. Hwang, Y. Cui, Z. Liu and Y. Zhang, *ACS Nano*, 2013, **7**, 8963–8971.
21 Y. Zhan, Z. Liu, S. Najmaei, P. M. Ajayan and J. Lou, *Small*, 2012, **8**, 966–971.
22 Y. Jung, J. Shen, Y. Liu, J. M. Woods, Y. Sun and J. J. Cha, *Nano Lett.*, 2014, **14**, 6842–6849.
23 C. M. Orofeo, S. Suzuki, Y. Sekine and H. Hibino, *Appl. Phys. Lett.*, 2014, **105**, 083112.
24 J. Park, N. Choudhary, J. Smith, G. Lee, M. Kim and W. Choi, *Appl. Phys. Lett.*, 2015, **106**, 012104.
25 A. Tarasov, P. M. Campbell, M.-Y. Tsai, Z. R. Hesabi, J. Feirer, S. Graham, W. J. Ready and E. M. Vogel, *Adv. Funct. Mater.*, 2014, **24**, 6389–6400.
26 J. Wang, L. Chen, W. Lu, M. Zeng, L. Tan, F. Ren, C. Jiang and L. Fu, *RSC Adv.*, 2015, **5**, 4364–4367.
27 J. R. Brent, N. Savjani and P. O'Brien, *Prog. Mater. Sci.*, 2017, **89**, 411–478.
28 E. Varrla, K. R. Paton, C. Backes, A. Harvey, R. J. Smith, J. McCauley and J. N. Coleman, *Nanoscale*, 2014, **6**, 11810–11819.
29 K. R. Paton, E. Varrla, C. Backes, R. J. Smith, U. Khan, A. O'Neill, C. Boland, M. Lotya, O. M. Istrate, P. King, T. Higgins, S. Barwich, P. May, P. Puczkarski, I. Ahmed, M. Moebius, H. Pettersson, E. Long, J. a. Coelho, S. E. O'Brien, E. K. McGuire, B. M. Sanchez, G. S. Duesberg, N. McEvoy, T. J. Pennycook, C. Downing, A. Crossley, V. Nicolosi and J. N. Coleman, *Nat. Mater.*, 2014, **13**, 624–630.
30 E. Varrla, C. Backes, K. R. Paton, A. Harvey, Z. Gholamvand, J. McCauley and J. N. Coleman, *Chem. Mater.*, 2015, **27**, 1129–1139.
31 N. Liu, P. Kim, J. H. Kim, J. H. Ye, S. Kim and C. J. Lee, *ACS Nano*, 2014, **8**, 6902–6910.
32 J. N. Coleman, M. Lotya, A. O'Neill, S. D. Bergin, P. J. King, U. Khan, K. Young, A. Gaucher, S. De, R. J. Smith, I. V. Shvets, S. K. Arora, G. Stanton, H.-Y. Kim, K. Lee, G. T. Kim, G. S. Duesberg, T. Hallam, J. J. Boland, J. J. Wang, J. F. Donegan, J. C. Grunlan, G. Moriarty, A. Shmeliov, R. J. Nicholls, J. M. Perkins, E. M. Grieveson, K. Theuwissen, D. W. McComb, P. D. Nellist and V. Nicolosi, *Science*, 2011, **331**, 568–571.
33 R. J. Smith, P. J. King, M. Lotya, C. Wirtz, U. Khan, S. De, A. O'Neill, G. S. Duesberg, J. C. Grunlan, G. Moriarty, J. Chen, J. Wang, A. I. Minett, V. Nicolosi and J. N. Coleman, *Adv. Mater.*, 2011, **23**, 3944–3948.
34 P. May, U. Khan, J. M. Hughes and J. N. Coleman, *J. Phys. Chem. C*, 2012, **116**, 11393–11400.
35 G. Cunningham, M. Lotya, C. S. Cucinotta, S. Sanvito, S. D. Bergin, R. Menzel, M. S. P. Shaffer and J. N. Coleman, *ACS Nano*, 2012, **6**, 3468–3480.
36 Y. Yao, Z. Lin, Z. Li, X. Song, K.-S. Moon and C.-p. Wong, *J. Mater. Chem.*, 2012, **22**, 13494–13499.
37 V. Nicolosi, M. Chhowalla, M. G. Kanatzidis, M. S. Strano and J. N. Coleman, *Science*, 2013, **340**, 1226419.

38 M. Mohiuddin, Y. Wang, A. Zavabeti, N. Syed, R. S. Datta, H. Ahmed, T. Daeneke, S. P. Russo, A. R. Rezk, L. Y. Yeo and K. Kalantar-Zadeh, *Chem. Mater.*, 2018, **30**, 5593–5601.
39 U. Khan, A. O'Neill, M. Lotya, S. De and J. N. Coleman, *Small*, 2010, **6**, 864–871.
40 U. Khan, H. Porwal, A. O'Neill, K. Nawaz, P. May and J. N. Coleman, *Langmuir*, 2011, **27**, 9077–9082.
41 A. O'Neill, U. Khan and J. N. Coleman, *Chem. Mater.*, 2012, **24**, 2414–2421.
42 N. Savjani, E. A. Lewis, R. A. D. Pattrick, S. J. Haigh and P. O'Brien, *RSC Adv.*, 2014, **4**, 35609–35613.
43 V. Forsberg, R. Zhang, J. Bäckström, C. Dahlström, B. Andres, M. Norgren, M. Andersson, M. Hummelgård and H. Olin, *PLoS One*, 2016, **11**, e0154522.
44 H. Ma, Z. Shen and S. Ben, *J. Colloid Interface Sci.*, 2018, **517**, 204–212.
45 S. M. Notley, *Langmuir*, 2012, **28**, 14110–14113.
46 K.-G. Zhou, N.-N. Mao, H.-X. Wang, Y. Peng and H.-L. Zhang, *Angew. Chem., Int. Ed.*, 2011, **50**, 10839–10842.
47 J. Kim, S. Kwon, D.-H. Cho, B. Kang, H. Kwon, Y. Kim, S. O. Park, G. Y. Jung, E. Shin, W.-G. Kim, H. Lee, G. H. Ryu, M. Choi, T. H. Kim, J. Oh, S. Park, S. K. Kwak, S. W. Yoon, D. Byun, Z. Lee and C. Lee, *Nat. Commun.*, 2015, **6**, 8294.
48 O. Y. Posudievsky, O. A. Khazieieva, V. V. Cherepanov, G. I. Dovbeshko, A. G. Shkavro, V. G. Koshechko and V. D. Pokhodenko, *J. Mater. Chem. C*, 2013, **1**, 6411–6415.
49 C. Campbell, *J. Acoust. Soc. Am.*, 1991, **89**, 1479–1480.
50 J. Friend and L. Yeo, *Rev. Mod. Phys.*, 2011, **83**, 647–704.
51 H. Ahmed, A. R. Rezk, B. J. Carey, Y. Wang, M. Mohiuddin, K. J. Berean, S. P. Russo, K. Kalantar-zadeh and L. Y. Yeo, *Adv. Mater.*, 2018, **30**, 1704756.
52 S. Marqus, H. Ahmed, M. Ahmed, C. Xu, A. R. Rezk and L. Y. Yeo, *ACS Appl. Nano Mater.*, 2018, **1**, 2503–2508.
53 L. Y. Yeo and J. R. Friend, *Biomicrofluidics*, 2009, **3**, 012002.
54 L. Y. Yeo and J. R. Friend, *Annu. Rev. Fluid Mech.*, 2014, **46**, 379–406.
55 G. Destgeer and H. J. Sung, *Lab Chip*, 2015, **15**, 2722–2738.
56 S. Gražulis, D. Chateigner, R. T. Downs, A. F. T. Yokochi, M. Quiros, L. Lutterotti, E. Manakova, J. Butkus, P. Moeck and A. Le Bail, *J. Appl. Crystallogr.*, 2009, **42**, 726–729.
57 S. Gražulis, A. Daškevič, A. Merkys, D. Chateigner, L. Lutterotti, M. Quirós, N. R. Serebryanaya, P. Moeck, R. T. Downs and A. Le Bail, *Nucleic Acids Res.*, 2012, **40**, D420–D427.
58 R. G. Dickinson and L. Pauling, *J. Am. Chem. Soc.*, 1923, **45**, 1466–1471.
59 M. Miansari, A. Qi, L. Y. Yeo and J. R. Friend, *Adv. Funct. Mater.*, 2014, **25**, 1014–1023.
60 S. Bertolazzi, J. Brivio and A. Kis, *ACS Nano*, 2011, **5**, 9703–9709.
61 Z. X. Gan, L. Z. Liu, H. Y. Wu, Y. L. Hao, Y. Shan, X. L. Wu and P. K. Chu, *Appl. Phys. Lett.*, 2015, **106**, 233113.
62 H. Lin, C. Wang, J. Wu, Z. Xu, Y. Huang and C. Zhang, *New J. Chem.*, 2015, **39**, 8492–8497.
63 K. Sakano, M. K. Kurosawa and T. Shigematsu, *Adv. Robot.*, 2010, **24**, 1407–1421.
64 R. J. Shilton, N. R. Glass, P. Chan, L. Y. Yeo and J. R. Friend, *Appl. Phys. Lett.*, 2011, **98**, 254103.
65 A. Wixforth, C. Strobl, C. Gauer, A. Toegl, J. Scriba and Z. v. Guttenberg, *Anal. Bioanal. Chem.*, 2004, **379**, 982–991.
66 M. K. Tan, J. R. Friend and L. Y. Yeo, *Lab Chip*, 2007, **7**, 618–625.
67 A. Renaudin, E. Galopin, V. Thomy, C. Druon and F. Zoueshtiagh, *Phys. Fluids*, 2007, **19**, 091111.
68 P. Brunet, M. Baudoin, O. B. Matar and F. Zoueshtiagh, *Phys. Rev. E: Stat., Nonlinear, Soft Matter Phys.*, 2010, **81**, 036315.
69 M. Baudoin, P. Brunet, O. Bou Matar and E. Herth, *Appl. Phys. Lett.*, 2012, **100**, 154102.
70 A. Bussonnière, M. Baudoin, P. Brunet and O. B. Matar, *Phys. Rev. E: Stat., Nonlinear, Soft Matter Phys.*, 2016, **93**, 053106.
71 Y. Chen, X. Ding, S.-C. Steven Lin, S. Yang, P.-H. Huang, N. Nama, Y. Zhao, A. A. Nawaz, F. Guo, W. Wang, Y. Gu, T. E. Mallouk and T. J. Huang, *ACS Nano*, 2013, **7**, 3306–3314.
72 A. R. Rezk, B. Carey, A. F. Chrimes, D. W. M. Lau, B. C. Gibson, C. Zheng, M. S. Fuhrer, L. Y. Yeo and K. Kalantar-zadeh, *Nano Lett.*, 2016, **16**, 849–855.
73 A. R. Rezk, S. Walia, R. Ramanathan, H. Nili, J. Z. Ou, V. Bansal, J. R. Friend, M. Bhaskaran, L. Y. Yeo and S. Sriram, *Adv. Opt. Mater.*, 2015, **3**, 888–894.